JOURNAL OF GEOPHYSICAL RESEARCH, VOL. 103, NO. C10, PAGES 21,601–21,609, SEPTEMBER 15, 1998

Spectral reflectance and absorption of a massive red tide off southern California

Mati Kahru and B. Greg Mitchell

Scripps Institution of Oceanography, University of California San Diego, La Jolla

Abstract. Spectral reflectance and absorption of a massive *Lingulodinium (Gonyaulax) polyedra* red tide in March 1995 off southern California are compared to a "baseline" of bio-optical measurements from the California Cooperative Oceanic Fisheries Investigations. The red tide was characterized by increased absorption and therefore reduced remote sensing reflectance (R_{rs}) in the 340-400 nm spectral range. The increased ultraviolet absorption was probably caused by mycosporine-like amino acids in the particulate fraction as well as increased absorption by dissolved organic matter. The chlorophyll *a* (chl *a*) specific particulate absorption of the *L. polyedra* bloom in the visible spectral range remained relatively constant for the chl a range 1-150 mg m^{-3} indicating accumulation of cells with similar optical characteristics. The difference in the R_{rs} versus chl *a* relationship of the red tide and "normal" California Current phytoplankton diminished with increasing wavelength from 340 nm and disappeared at 412 nm. Ratios of R_{rs} at 340 nm (or 380 nm) and 412 nm (or 443 nm) provided differentiation of the red tide starting at chl *a* concentration of 1-2 mg m^{-3}. The forthcoming Japanese Global Imager (GLI) satellite sensor has, among others, the 380 nm band. If the signal to noise ratio and atmospheric correction for the 380 nm band are sufficient to retrieve the dynamic range of the water leaving radiance, then it might be possible to differentiate red tides from other phytoplankton blooms with the algorithm described here.

1. Introduction

Red tides, i.e., massive dinoflagellate blooms causing water discoloration, are an increasingly important problem in many coastal environments [e.g., *Anderson*, 1995]. Some of the red tide organisms are toxic to other biota and can cause significant economic losses. Even a nontoxic red tide can be a dramatic and undesirable disturbance to the ecosystem, and in shallow or enclosed waters the bloom's demise can result in anoxia. Remote detection and monitoring of red tides from satellites and/or aircraft are therefore important challenges to modern oceanography.

In the spring of 1995 the coast of southern California experienced a massive red tide that started in March as a bloom of a dinoflagellate *Lingulodinium polyedra* and was followed in April by a bloom of a heterotrophic dinoflagellate *Noctiluca scintillans*. Similar blooms of *Lingulodinium polyedra* (formerly known as *Gonyaulax polyedra*) have been reported in southern California every few years since at least 1901 [*Torrey*, 1902; *Allen*, 1946; *Holmes et al.*, 1967]. The 1995 bloom was probably exceptional in its magnitude. In a 15-year time series of chlorophyll *a* (chl *a*) concentration from the Scripps Pier, the highest value before the 1995 bloom was 50 mg m^{-3} (J. McGowan, unpublished data, 1995). In the 1995 *L. polyedra* bloom, surface chl *a* exceeded concentrations of 100 mg m^{-3}, with one observation of 500 mg m^{-3}. Dinoflagellate cell concentrations of up to 20 x 10^6 and chl *a* up to 500 mg m^{-3} have been also reported in the mid-1960s in this area [*Holmes et al.*, 1967].

The fact that red tides alter the bio-optical properties of water bodies is obvious from the very definition of red tides as a change in water color. However, the quantitative relationships between in situ biological and bio-optical quantities and remotely observable quantities of red tides have not been described. Ocean color is usually understood in terms of the remote sensing reflectance, which is defined as the ratio of the upwelling radiance (L_u) and downwelling irradiance (E_d) and can be approximated as a function of the ratio of the backscattering coefficient b_b and absorption coefficient a [e.g., *Gordon et al.*, 1988]:

$$R_{rs}(\lambda) = L_u(\lambda) / E_d(\lambda) = c \times b_b(\lambda) / a(\lambda) \qquad (1)$$

(see notation section for symbol definitions). Here $b_b(\lambda)$ is expected to be relatively flat for large cells like *L. polyedra* and $a(\lambda)$ with its strong spectral structure should control the "ocean color." The term represented here by c is actually a complex function of the viewing geometry, incident radiance distribution and anisotropic optical properties of the water body [*Morel and Gentili*, 1991, 1996]. Typically, upper layer quantities, such as chl *a*, are estimated from ratios of $R_{rs}(\lambda)$ at two wavelengths as this eliminates most of the environmental and geometric variability embedded in the term c of (1) [*Gordon and Morel*, 1983; *Gordon et al.*, 1988; *Morel and Gentili*, 1996]:

$$chl\ a = A_{12} [R_{rs}(\lambda_1) / R_{rs}(\lambda_2)]^{-B_{12}}, \qquad (2)$$

where A_{12} and B_{12} are coefficients corresponding to wave-

Paper number 98JC01945.
0148-0227/98/98JC-01945$09.00

lengths λ_1 and λ_2. For estimating chl *a* the first wavelength λ_1 is usually taken at or near the chl *a* blue absorption maximum at 443 nm and λ_2 is from the low chl *a* absorption region around 555 nm. Even ratios with λ_1 outside the chl *a* absorption maximum (e.g. at 490 nm) are highly correlated with chl *a* due to the strong correlation between accessory pigments absorbing at 490 nm and chl *a* [*Aiken et al.*, 1995]. The dominant patterns in the observed R_{rs} and R_{rs} ratios can be explained by changes in the absorption and backscattering coefficients (1). Experimental measurements and modeling studies [*Ahn et al.*, 1992] show that under most conditions values of $b_b(\lambda)$ are small, decrease monotonically with respect to wavelength, and are dominated by particles < 1 μm in size. However, b_b becomes an important part of the R_{rs} variation in blooms of coccolithophores [*Balch et al.*, 1991], cyanobacteria *Trichodesmium* [*Borstad et al.*, 1992] and *Nodularia* [*Kahru et al.*, 1994]. As a good approximation for ocean areas void of phytoplankton surface accumulations and coccolithophore blooms, we may therefore assume that changes in R_{rs} ratios at two wavelengths are dominated by changes in $a(\lambda)$. The absorption coefficient for natural waters is comprised of the components due to pure seawater, $a_w(\lambda)$, particulates, $a_p(\lambda)$, and dissolved materials, $a_s(\lambda)$:

$$a(\lambda) = a_w(\lambda) + a_p(\lambda) + a_s(\lambda) \quad (3)$$

Analyzing an extensive set of particulate absorption spectra, which are a dominant part of total variation in absorption and therefore R_{rs} ratios, *Garver et al.* [1994] found that the variability in $a_p(\lambda)$ between 400-700 nm was almost entirely associated with the quantity of the absorbing materials rather than their spectral quality. *Garver et al.* [1994] concluded that development of algorithms for distinguishing particular phytoplankton groups (e.g., diatoms and dinoflagellates) from remotely sensed ocean color spectra appeared unlikely.

Here we show that by extending the study of $a_p(\lambda)$ and $R_{rs}(\lambda)$ into the ultraviolet (UV) region (340-380 nm) the remote detection of red tides is possible. We do this by comparing the bio-optical characteristics measured during the 1995 red tide to a large "baseline" data set of bio-optical measurements from the California Cooperative Oceanic Fisheries Investigations (CalCOFI). Reduced reflectance in the UV is presumably due to the strong absorption of the mycosporine-like amino acids (MAAs) that are present in the red tide dinoflagellates. The Japanese ADEOS-II spacecraft will include the Global Imager (GLI) with a wavelength band centered at 380 nm as well as the more traditional ocean color bands. Thus the detection and monitoring of red tides by satellite remote sensing may become feasible.

2. Data and Methods

The bio-optical characteristics of the red tide are evaluated by comparing the data sets collected with identical instrumentation and very similar methods from a massive red tide event and the regular CalCOFI cruises in the California Current area. The data collected off the Scripps Pier (March 8, 1995) and from a cruise RED9503 (11 stations, March 28-30, 1995) during the *L. polyedra* bloom are collectively referred to as the red tide data set. The CalCOFI grid and the red tide stations are shown in Figure 1. The CalCOFI bio-optical data set represents a total of sixteen CalCOFI cruises completed

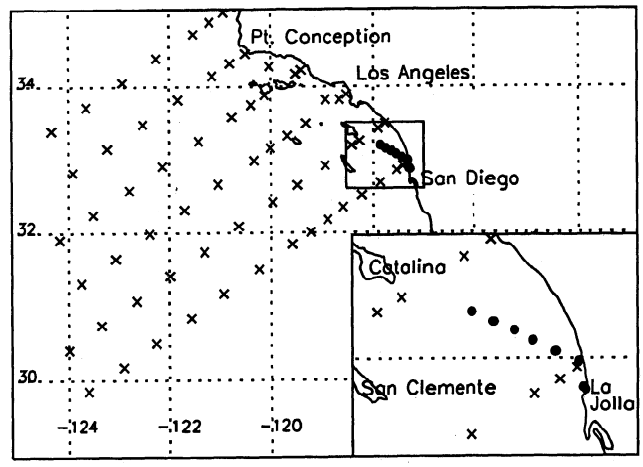

Figure 1. Map of the regular CalCOFI stations (crosses) and the red tide stations (filled circles and inset). The red tide stations start from the Scripps Pier and extend northwest.

between August 1993 and October 1997, with over 300 coincident bio-optical profiles, particulate absorption, and surface pigment measurements [*Mitchell and Kahru*, 1998]. Measurements of absorption by the dissolved organic matter are available for some cruises since 1995.

Vertical profiles of downwelling spectral irradiance, E_d, and upwelling radiance, L_u, at 12 wavelength bands between 340 and 665 nm were measured with an underwater MER-2040 radiometer (Biospherical Instruments Inc.). Above-water incident spectral irradiance E_s was measured simultaneously with a mast-mounted spectroradiometer MER-2041 at 12 wavelength bands between 340 and 885 nm. A detailed radiometric calibration history of the instruments is available [*Mitchell and Kahru*, 1998]. The profiling procedures were in accordance with sea-viewing wide-field-of-view-sensor (SeaWiFS) bio-optical protocols [*Mueller and Austin*, 1995] and are described in *Mitchell and Kahru* [1998].

Processing of the bio-optical profiles was done with a modified version of the Bermuda Bio-Optics Project (BBOP) data processing system [*Siegel et al.*, 1995; *Mitchell and Kahru*, 1998]. The vertical profiles were sampled into bins of a constant depth increment. The binning interval was 1 m for the CalCOFI data and either 25 or 75 cm (depending on the station depth and attenuation coefficient) for the red tide data. The depths of the different variables were adjusted according to the position of the particular sensor in relation to the depth sensor. Binning to depth intervals < 1 m was essential for processing the red tide profiles with very high attenuation.

$L_u(\lambda)$ measured by an instrument of a finite size is affected by the instrument's own shadow. As shown by theoretical calculations [*Gordon and Ding*, 1992] and measurements [*Zibordi and Ferrari*, 1995], this error can be satisfactorily corrected if the product of the total absorption coefficient times the radius of the instrument is below a certain limit. The self-shading correction scheme based on *Gordon and Ding* [1992] and recommended by *Mueller and Austin* [1995] was used here. The total absorption coefficient $a(\lambda)$ was estimated as $0.7*K_{Ed}(\lambda)$, where 0.7 is the mean cosine of the radiance field for the upper ocean. The estimate of the mean cosine is based on our measurements and is consistent with theoretical

calculations [*Kirk*, 1991]. The ratio of the diffuse skylight to direct sunlight was assumed to be 0.43 for the red tide data, corresponding to 70% direct and 30% diffuse irradiance for the very clear skies during the cruise (R. Frouin, personal communication, 1997). The corrections of $L_u(\lambda)$ were significant (up to 34.2% at 340 nm) for the red tide data and for the CalCOFI data with high chl *a* concentration. The median correction for self-shading for the CalCOFI data was 3.9% at 340 nm (lower in the visible range), while the maximum correction was 25.8% at 340 nm and between 10 and 15% in the visible. The red tide station with the highest absorption (163 mg m^{-3} of chl *a*) was beyond the correction range of *Gordon and Ding* [1992] and was excluded.

For calculating the remote sensing reflectance just above the sea surface, $R_{rs}(0^+, \lambda)$, the following equation was used for the CalCOFI data:

$$R_{rs}(0^+, \lambda) = 0.54\, L_u(0^-, \lambda)/[1.04\, E_d(0^-, \lambda)]. \quad (4)$$

Here $L_u(0^-, \lambda)$ is the upwelling radiance extrapolated to just below the sea surface, $E_d(0^-, \lambda)$ is the downwelling irradiance extrapolated to just below the sea surface and the coefficients 0.54 and 1.04 are the transfer coefficients of the air-sea interface for L_u and E_d, respectively [*Austin*, 1974]. For the red tide data $R_{rs}(0^+, \lambda)$ was calculated directly from the incident (surface) irradiance:

$$R_{rs}(0^+, \lambda) = 0.54\, L_u(0^-, \lambda) / E_s(\lambda) \quad (5)$$

While both (4) and (5) gave similar results for the CalCOFI data set [*Mitchell and Kahru*, 1998], (4) was preferred for the CalCOFI data because of smaller variability and because of missing E_s data on some cruises. Equation 5 was preferred for the red tide data due to larger errors of estimating $E_d(0^-, \lambda)$ for stations with very strong light attenuation and strong vertical gradient in the near-surface chl *a* concentration. Increased variance of (5) when applied to the CalCOFI data is primarily attributed to surface phenomena such as ship shadowing and wave focusing, which affect both E_d and L_u on the underwater unit but not E_s on the above-water unit. Time and space offsets when shadows from clouds or the ship's superstructure affect the above- and in-water sensors differently also contribute to the variance of (5). In the red tide case these considerations were of minor importance, in part because of the clear skies, low winds, and very smooth surface wave conditions.

The chl *a* and phaeopigment concentrations for the CalCOFI data were determined by the Marine Life Research Group (MLRG) of Scripps Institution of Oceanography using the fluorometric method [*Holm-Hansen et al.*; 1965; *Venrick and Hayward*, 1984]. For the red tide data set we used the MLRG procedure and their fluorometer to ensure consistent results.

Absorption by particulate matter was measured according to procedures outlined by *Mitchell* [1990]. Water samples were filtered onto Whatman GF/F filters, which were placed on quartz holders in a spectrophotometer. A blank GF/F filter, saturated with 0.2 μm filtered seawater, was used as reference. Absorption coefficients for the CalCOFI samples were calculated using the path-length amplification factor, β, of *Mitchell* [1990]. The *Mitchell* [1990] β is based on the quadratic function and is optimized for filter optical density, OD_f, between 0.05 and 0.4. At higher OD_f values, such as those obtained from the red tide samples, the *Mitchell* [1990] function is not appropriate; it becomes < 1.0 at $OD_f \approx 0.9$, which is physically unrealistic. A power function was fit to the same data set used by *Mitchell* [1990] with the result:

$$\beta = 1.22\, OD_f^{-0.254} \quad (6)$$

A few experiments showed that the power function provided better reproducibility for the multiple volume filtrations of the red tide samples (15% mean coefficient of variation versus more than 35% with the *Mitchell* [1990] β function). Both functions produced similar results for OD_f in the range 0.1-0.4.

Absorption by dissolved organic substances was measured from 300-800 nm in a dual beam spectrophotometer using Millipore Milli-Q water in the reference beam following *Mueller and Austin* [1995]. For the red tide data we used a Perkin Elmer Lambda 6 and for the CalCOFI we used a Varian Cary 1 spectrophotometer. Quartz cuvettes (10 cm pathlength and 2.5 cm diameter) were used for the sample and reference water. Sample water was filtered using 0.2 μm polycarbonate filters to remove particles. The filters were prerinsed 3 times with ~10-20 ml of Milli-Q water for each rinse. The prerinse is essential to remove material from the filters that has absorption similar to that of dissolved organic matter absorption. Raw sample absorbance measured relative to the Milli-Q reference was normalized to zero at 600 nm due to temperature-dependent artifacts [*Pegau and Zaneveld*, 1993] observed between 650-750 nm. Raw absorbances were then multiplied by 2.303 to convert from $\log_{10}$ to $\log_e$ and by 10 to convert to a 1 m pathlength.

3. Results

3.1. Remote Sensing Reflectance

All possible combinations of (2) with λ_1 and λ_2 from the set of SeaWiFS wavelengths (412, 443, 490, 510, 555, and 665 nm) as well as 532 and 570 nm were tested for the possibility of detecting the magnitude of the *L. polyedra* bloom and/or chl *a* concentration. While many ratios showed high correlation with estimates of plant biomass (chl *a*), none allowed discrimination between the dinoflagellate dominated red tide and high chl *a* upwelling waters off California dominated by diatoms; none of the R_{rs} versus chl *a* relationships were significantly different (at 90% confidence level) between the CalCOFI and red tide data sets. Reflectance ratios at some λ_1 and λ_2 combinations that are commonly used to estimate chl *a* (2) are shown in Figure 2. Large errors are inevitable when standard ocean color algorithms are applied to areas affected by red tides. The operational SeaWiFS algorithm (OC2) uses modified cubic polynomial of the $R_{rs}(490)/R_{rs}(555)$ ratio to estimate chl *a* [*O'Reilly et al.*, 1998]. At high chl *a* concentration the sigmoid shape of the algorithm becomes extremely sensitive to small variations in $R_{rs}(490)/R_{rs}(555)$ and, for our red tide data, results in overestimating the measured chl *a* values by an order of magnitude. The data set used to develop the OC2 algorithm included very few chl *a* values over 10 mg m^{-3} and none from red tides.

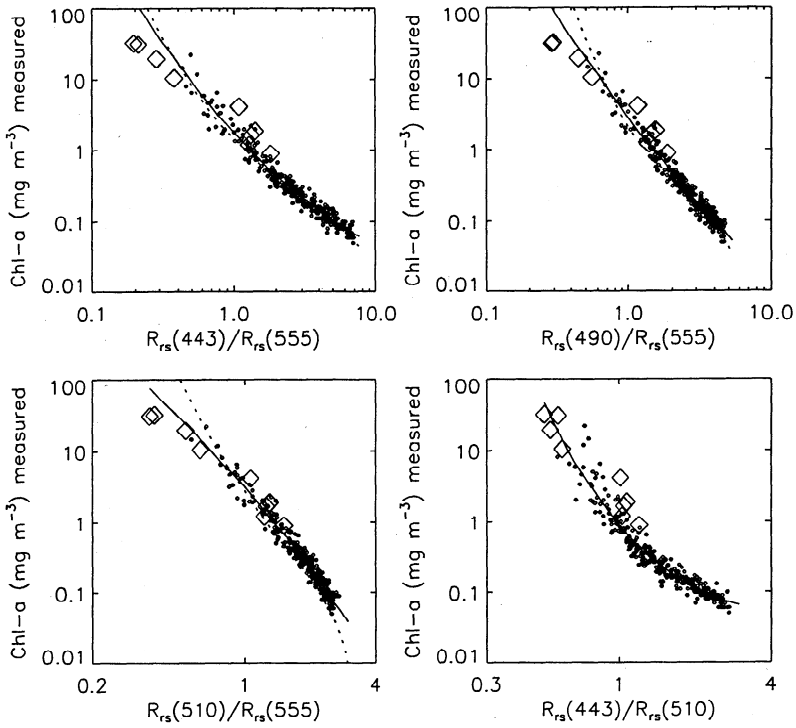

Figure 2. Near-surface chl *a* concentration as a function of reflectance ratios of various SeaWiFS bands: $R_{rs}(443)/R_{rs}(555)$, $R_{rs}(490)/R_{rs}(555)$, $R_{rs}(510)/R_{rs}(555)$, and $R_{rs}(443)/R_{rs}(510)$. Simple cubic regressions (solid lines) were fitted to the CalCOFI data (small diamonds). The red tide data (large diamonds) were not used in the regressions. Respective global Ocean Color 2 algorithms [*O'Reilly et al.*, 1998] are shown as dotted curves.

The red tide samples form two clusters: those with moderate chl *a* concentration (< 10 mg m^{-3}) and those with high chl *a* (> 10 mg m^{-3}). The two clusters tend to be on the opposite sides of the CalCOFI regression line. Hereafter, we refer to those clusters as the low-bloom and the high-bloom samples. The distributions of the red tide and CalCOFI data sets overlap considerably, precluding discrimination between the red tide and CalCOFI stations using R_{rs} ratios in the 412-570 nm spectral region.

The red tide samples had significant differentiation when reflectances in the ultraviolet part of the spectrum were evaluated relative to chl *a*. The R_{rs} values in the 340 nm and 380 nm bands, in particular, were significantly lower at high chl *a*, and the difference with the CalCOFI data decreased monotonically with increasing wavelength from 340 nm to 412 nm (Figure 3). The relationship between R_{rs} and chl *a* for the CalCOFI data changed slope (at ~0.3 mg m^{-3}) and became flatter at higher chl *a*. This effect was more evident at shorter wavelengths. At 395 nm and longer wavelengths the regressions for the two data sets were not distinguishable at the 90% confidence level. Therefore using a reflectance ratio with one wavelength in the region of the large difference (340 or 380 nm) and another in the region of small or no difference (412 or 443 nm) provides a method to differentiate red tide data from the CalCOFI data. Reflectance ratios with λ_1 = 340 nm (Figures 4a and 4b) seemed to differentiate the red tide stations from the bulk of the CalCOFI data down to chl *a* values of ~1 mg m^{-3}. Replacing 340 nm with 380 nm (Figures 4c and 4d) resulted in some loss of the separation capability at lower chl *a* but produced equally good separation at chl *a* > 2 mg m^{-3}. A few CalCOFI data points showing low values of $R_{rs}(340)/R_{rs}(412)$ and $R_{rs}(380)/R_{rs}(412)$ and similar to the low-bloom red tide data were near-shore stations of the two southernmost CalCOFI lines (Figure 1). For the CAL9504 cruise those data points actually measured the same red tide event a week after the RED9503 cruise. It is likely that these stations were influenced by the presence of high dinoflagellate concentrations on other cruises as well.

3.2. Particulate Absorption

Chlorophyll *a* specific absorption spectra ($a^*_{p\,chl}(\lambda)$ = $a_p(\lambda)/chl\ a$) averaged over a range of chl *a* values are shown in Figure 5. In the 400-700 nm range the CalCOFI spectra show the well-known progressive decrease in $a^*_{p\,chl}$ with increasing chl *a*. This decrease in the specific absorption is due to increased pigment packaging at high chl *a* and increased relative absorption by detritus and photoprotective pigments at low chl *a* [*Mitchell and Kiefer*, 1988; *Bricaud et al.*, 1995; *Sosik and Mitchell*, 1995]. When only the blue to green ratio is considered, the red tide $a^*_{p\,chl}$ data look similar to the CalCOFI $a^*_{p\,chl}$ data extrapolated to high chl *a*. However, in the 300-380 nm range, the $a^*_{p\,chl}$ values of the red tide data, especially the high-bloom samples, are significantly higher compared to the CalCOFI data at high chl *a*. Moreover, between 300 and 400 nm, $a^*_{p\,chl}$ did not decrease but even increased from the low-bloom samples to high-bloom samples, which is contrary to the generally observed trend of decreasing $a^*_{p\,chl}$ at higher chl *a* (Figure 5).

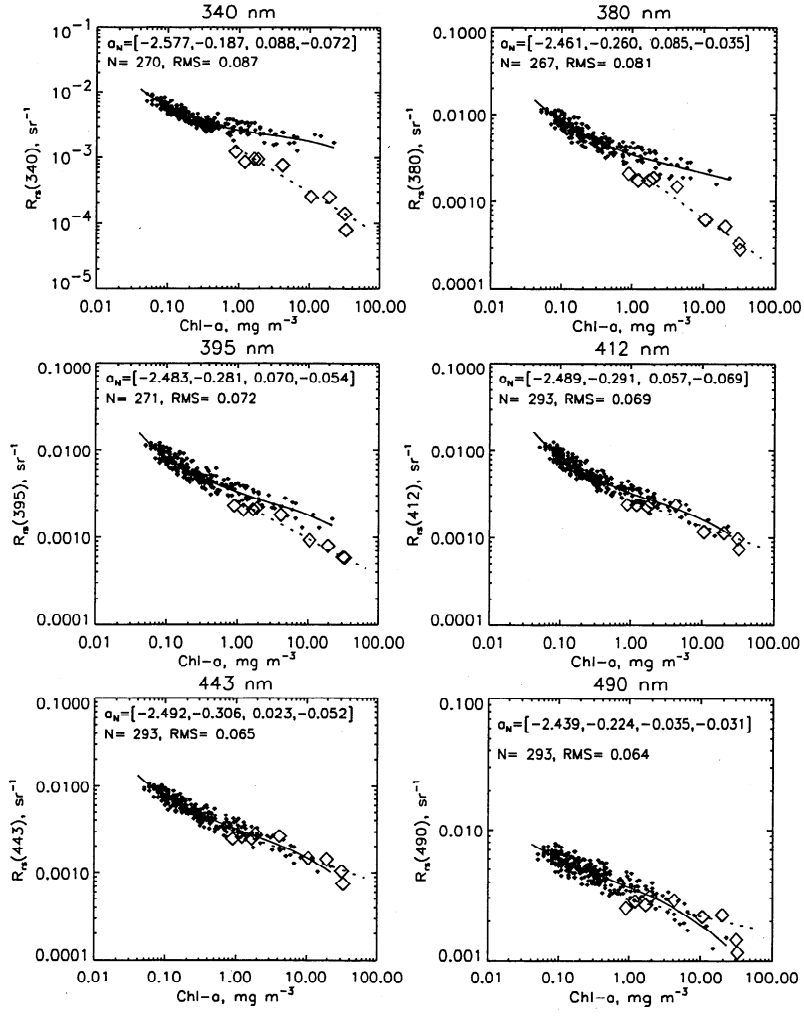

Figure 3. Remote sensing reflectance R_{rs} as a function of chl *a* concentration for the CalCOFI (small diamonds) and the red tide (large diamonds) data sets. Solid line is the cubic regression fit to the CalCOFI data (in log-log space) with the values of the polynomial coefficients (a_0 to a_3) given in the inset. The number of samples used (N) and the root mean square error of the estimate (RMS) are given. The dashed line is the robust linear regression line for the red tide.

Scatterplots of $a_p(440)$ as a function of chl *a* (Figure 6) show that at comparable chl *a* levels the low-bloom red tide samples had lower a_p, indicating higher pigment packaging. High pigment packaging is probably caused by the large cell size (~50 μm) of *L. polyedra*. However, a_p for the red tide increased linearly for the range of chl *a* of 1-150 mg m^{-3}, resulting in higher a_p at high chl *a*, compared to the CalCOFI samples extrapolated to the same chl *a* concentration with a power function. The fact that $a^*_{p\ chl}$ remained relatively constant for the range of chl *a* spanning more than 2 orders of magnitude indicates increased concentration of cells with similar optical properties, rather than further increase in pigment packaging.

3.3. Absorption by Dissolved Material

We evaluated the contribution of the colored dissolved organic matter (CDOM) that also absorbs strongly in the UV as a possible cause for the decreased R_{rs} in the UV. The average $a_s(340)$ for the red tide low-bloom samples was approximately double the average $a_s(340)$ for the CalCOFI samples at similar chl *a* concentrations. Furthermore, the surface values of $a_s(340)$ were approximately 2 times higher than $a_p(340)$ for the low-bloom samples. While $a_s(340)$ approximately doubled from the low-bloom samples to the high-bloom samples, the average particulate absorption increased more than 10 times. It is therefore likely that increased a_s did contribute to the reduced UV reflectance in the red tide while the changes from the low-bloom to high-bloom samples were dominated by the 10-fold increase in particulate absorption. The relatively high a_s for the red tide samples, compared to CalCOFI, may explain the lack of differentiation in R_{rs} at 412 and 443 nm (Figure 3), even though there was some evidence of differences in a_p between the red tide and CalCOFI at low chl *a* (Figure 6). Part of the elevated a_s in the UV for the red tide situation may have been caused by extracellular release of mycosporine-like amino acids [*Vernet and Whitehead*, 1996].

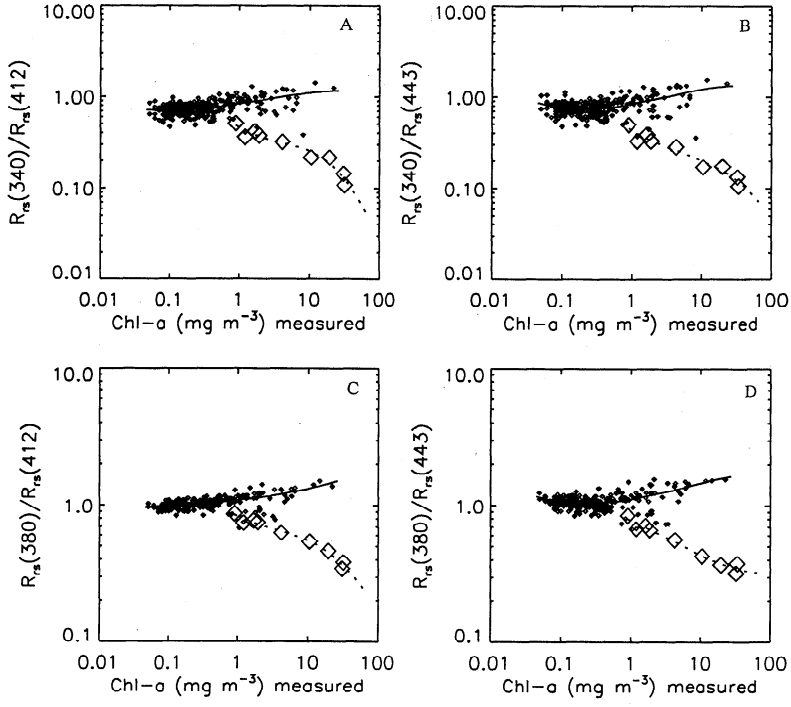

Figure 4. Reflectance ratios including UV bands as a function of chl *a* concentration for the CalCOFI (small diamonds and solid line) and red tide data (open diamonds and dotted line). The lines are cubic regression fits in the log-log space.

4. Discussion

We have shown that UV absorption characteristics of a red tide dominated by a dinoflagellate *L. polyedra* allow bio-optical differentiation of the red tide from typical conditions in southern California waters. The pigments in the moderate chl *a* (< 10 mg m^{-3}) red tide areas were highly packaged; that is, their chl *a* specific particulate absorption coefficient $a_p{}^*{}_{chl}$ in the 400-700 nm range was lower than for typical CalCOFI observations at corresponding chl *a*. However, a further increase in chl *a* by 2 orders of magnitude left $a_p{}^*{}_{chl}$ practically unchanged; that is, the absorption coefficient changed linearly with chl *a*. It is therefore hypothesized that variations in the chl *a* concentration in the surface waters of the red tide were caused by the variability in the cell concentration of *L. polyedra* with little variation in cellular optical properties in the visible range. Accumulation of dinoflagellates is possible as a result of interaction between their active vertical migration and current convergences in internal waves and eddies.

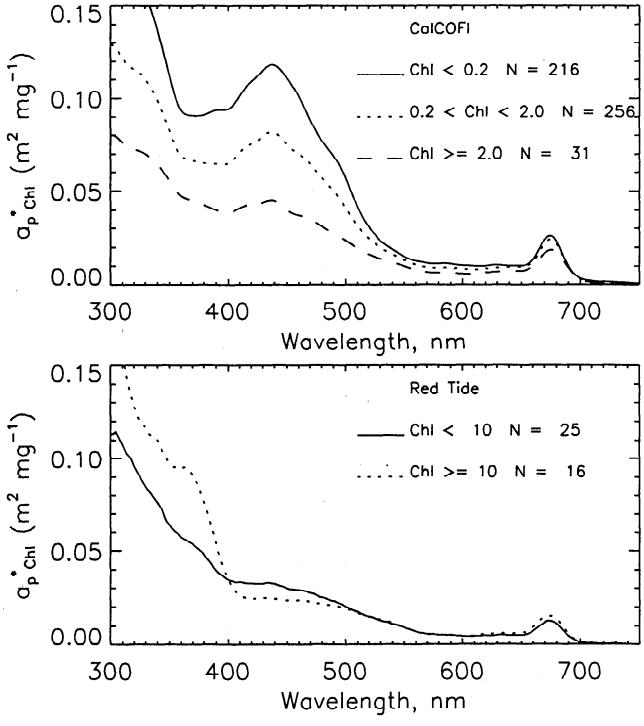

Figure 5. Average particulate absorption spectra normalized to chl *a* for three chl *a* ranges of the CalCOFI data (top) and two chl *a* ranges of the red tide data (bottom).

Garver et al. [1994] analyzed particulate absorption data from 400 to 700 nm and concluded that development of algorithms for distinguishing phytoplankton groups (e.g., diatoms and dinoflagellates) from remotely sensed ocean color spectra appeared unlikely. We have shown that a red tide dominated by a dinoflagellate *L. polyedra* can be differentiated from the CalCOFI baseline data set by using the increased absorption and thus reduced reflectance in the 300-400 nm spectral range. The anomalously high UV absorption was probably caused by MAAs [*Vernet and Whitehead*, 1996]. MAAs may provide direct photoprotection against UV inhibition of photosynthesis [*Dunlap et al.*, 1986; *Vernet et al.*, 1994; *Neale et al.*, 1997]. The reflectance ratio $R_{rs}(340)/R_{rs}(412)$ provided the best differentiation of the red tide stations from the regular CalCOFI samples, which are usually dominated by diatoms at high chl *a*. The difference in the R_{rs} between the red tide and the CalCOFI reference data set diminished with increasing wavelength from 340 to 412 nm. Using $R_{rs}(380)$ instead of $R_{rs}(340)$ in the reflectance ratio produced acceptable separation at chl *a* levels > 2 mg m^{-3}.

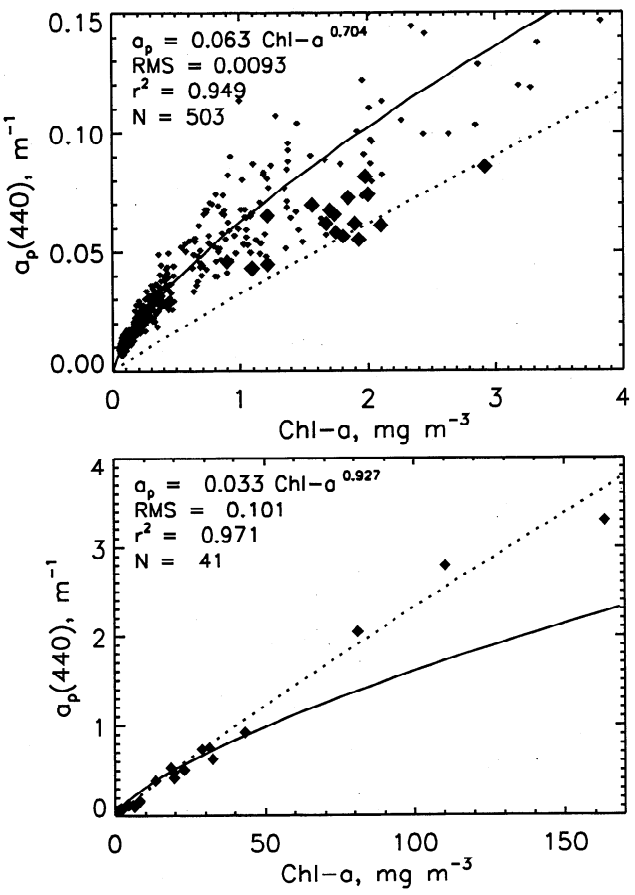

Figure 6. Absorption coefficient of particulate material at 440 nm as a function of chl *a* for the CalCOFI (small diamonds) and red tide (large filled diamonds) samples. Least squares fits of the power function to the CalCOFI data (top, solid lines) and red tide (bottom, dashed lines) are shown. (bottom) The red tide data in the full range is shown. The coefficient of determination (r^2), the root mean square error of the estimate (RMS) and the number of samples used (N) are given.

The detection of red tides by their MAA absorption may be complicated by interference of absorption by detrital and dissolved organic materials that also absorb strongly in the UV region. It has been shown [*Siegel and Michaels*, 1996] that the concentration of at least part of the colored dissolved materials do not covary with algal pigments even in the most oligotrophic environments. Laboratory studies of *L. polyedra* have shown that the cells not only synthesize MAAs but also excrete them into the environment [*Vernet and Whitehead*, 1996]. While absorption by dissolved organic materials (including MAAs) was important in the red tide samples with moderate chl *a*, particulate absorption completely dominated in the high-bloom red tide. As the shapes of absorption spectra of MAAs and typical dissolved organic materials are quite different, a general algorithm separating them should be possible.

More studies are needed before these observations of increased UV absorption (due to MAAs) in dinoflagellates can be considered sufficient to differentiate red tide dinoflagellates from other blooms. If the increased absorption in the UV of red tides proves to be generally valid and the R_{rs} ratios at 380 nm to 412 or 443 nm stay approximately similar for other species, then creating an operational algorithm is relatively straightforward. As a first approximation, values below a constant threshold value of 0.8 for $R_{rs}(380)/R_{rs}(412)$ and for chl $a > 1$ mg m^{-3} can be used to classify an area as a red tide (see Figure 4). Our algorithm of red tide detection could be tested immediately in geographically diverse red tide events using UV-visible reflectance instruments such as ours. It would also be straightforward to add UV sensors to existing airborne sensors if further in situ studies generalize our southern California bight observations.

An interesting task for bio-optical measurements would be to provide an estimate of the relative amounts of chl *a* contained in the red tide organisms versus the "regular" phytoplankton. Figure 7 shows a two-dimensional diagram where the horizontal axis varies with increasing chl *a* and vertical axis varies with increasing UV absorption. On this diagram a "regular" phytoplankton bloom, e.g., due to upwelling, would move a point to the right along the horizontal axis, while an intensifying red tide with relatively greater UV absorption would move a point diagonally up and right. Thus it is possible to use reflectance that can be estimated remotely to determine the presence of red tide dinoflagellates in the southern California bight.

Because of the relatively high absorption by both CDOM and particulate matter, the standard ocean color algorithms using either $R_{rs}(443)/R_{rs}(555)$ or $R_{rs}(490)/R_{rs}(555)$ will probably overestimate chl *a* when applied to areas with high-concentration red tides. In our case the operational SeaWiFS

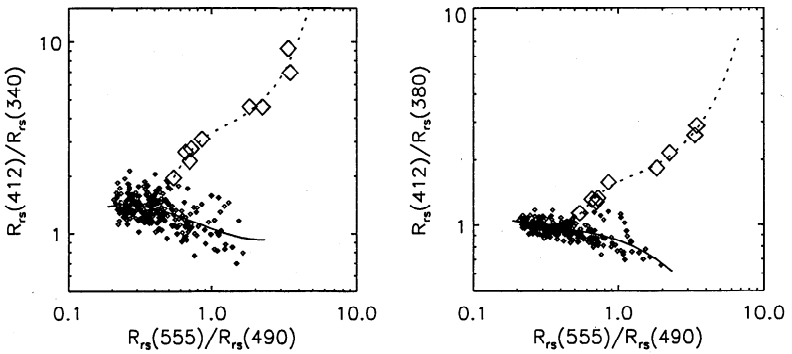

Figure 7. Two-dimensional scatter plots of $R_{rs}(412)/R_{rs}(340)$ and $R_{rs}(412)/R_{rs}(380)$ versus $R_{rs}(555)/R_{rs}(490)$ for the CalCOFI (small diamonds) and red tide (large diamonds) data. The horizontal axis corresponds to increasing chl *a*, and the vertical axis corresponds to increasing MAA absorption.

OC2 algorithm [*O'Reilly et al.*, 1998] overestimated chl *a* in the high-bloom stations by an order of magnitude.

Most satellite ocean color sensors of the past (Coastal Zone Color Scanner and Ocean Color Temperature Sensor) and present (SeaWiFS, Modular Optoelectronic Scanner), and near future (Moderate-resolution Imaging Spectrometer and Medium-resolution Imaging Spectrometer) do not possess bands below 400 nm and therefore cannot be used to detect red tides by their increased UV absorption. Also, the typical pixel size of ≈1 km^2 of these sensors limits their value for monitoring red tides in coastal zones.

The GLI satellite sensor to be launched on the ADEOS II spacecraft has, among others, wavelength bands at 380 and 400 nm that have not been available on any other ocean color satellite. GLI also has the 412 and 443 nm bands that are required to implement the red tide detection algorithm proposed here. If the signal to noise ratio of the 380 nm band after the atmospheric correction allows retrieval of the dynamic range of the water-leaving radiance, then it might be possible to use either $R_{rs}(380)/R_{rs}(412)$ or $R_{rs}(380)/R_{rs}(443)$ to detect red tides. Equivalently, the normalized water-leaving radiances L_{wn} can be used instead of R_{rs}. The presence of the 380 nm band, combined with the 250 m spatial resolution of some (spectrally wide) bands, makes the GLI a potentially powerful tool for monitoring coastal zones for algal blooms. While retrieval of the ocean reflectance in the UV may prove problematic for satellite sensors due to exponentially increasing Rayleigh scattering at shorter wavelengths, the concepts we present are usable immediately on profilers, moorings, and aircraft. Early detection and monitoring of harmful red tides is essential for mitigation. We hypothesize that UV reflectance will prove to be a useful tool for early detection and monitoring of certain types of dinoflagellate blooms.

Notation

$a(\lambda)$	total absorption coefficient of water, m^{-1}.
$a_p(\lambda)$	absorption coefficient of particulate matter, m^{-1}.
$a^*_{p\ chl}(\lambda)$	chl a specific particulate absorption coefficient, = $a_p(\lambda)$ chl *a*.
$a_s(\lambda)$	absorption coefficient of dissolved organic materials, m^{-1}.
$a_w(\lambda)$	absorption coefficient of pure sea-water, m^{-1}.
A_{12}, B_{12}	coefficients.
chl *a*	chlorophyll *a* or chlorophyll *a* concentration, mg m^{-3}.
$E_d(\lambda)$	downwelling spectral irradiance, W m^{-2} nm^{-1}.
$E_s(\lambda)$	incident surface irradiance above the sea surface, W m^{-2} nm^{-1}.
$E_d(0^-,\lambda)$	downwelling spectral irradiance just below the sea surface, W m^{-2} nm^{-1}.
$E_d(0^+,\lambda)$	downwelling spectral irradiance just above the sea surface, W m^{-2} nm^{-1}.
$K_{Ed}(\lambda)$	vertical attenuation coefficient for downwelled irradiance, m^{-1}.
$L_u(0^-,\lambda)$	upwelling spectral radiance just below the surface, W m^{-2} nm^{-1} sr^{-1}.
$L_u(0^+,\lambda)$	upwelling spectral radiance just above the surface, W m^{-2} nm^{-1} sr^{-1}.
$L_u(\lambda)$	upwelling spectral radiance, W m^{-2} nm^{-1} sr^{-1}.
$R_{rs}(\lambda)$	remote sensing reflectance, sr^{-1}.
$R_{rs}(0^+,\lambda)$	remote sensing reflectance just above the surface, sr^{-1}.
r^2	coefficient of determination.
OD_f	optical density of filter pad.
β	path-length amplification factor for light in filter pad.
$\lambda, \lambda_1, \lambda_2$	wavelengths, nm.

Acknowledgments. The CalCOFI work was supported by a grant from the NASA HQ Ocean Biogeochemistry Program and a cooperative agreement from NASA GSFC (NAGW-3665, NCC-5-48). The red tide cruise was supported by NOAA grant NA37GP0526 from the NOAA Coastal Ocean program. Analysis of UV reflectance was supported by NASDA grant G-0020 in support of GLI algorithm development. We thank Tiffany Moisan for chl *a* measurements for the red tide data set, P.J.S. Franks for many helpful discussions, David Siegel for making the BBOP software available, the CalCOFI Committee of UCSD and the NOAA SWFSC for encouraging our participation in the CalCOFI cruises; the CalCOFI technicians for extraordinary analytical and data reduction effort and for their provision of the CalCOFI data sets, Robert Knox and the SIO Marine Operations Committee for providing 2 days of time on the R/V Sproul for the RED9503 cruise, the SIO Marine Facility and Resident Technicians for assistance in configuring winches and laboratory vans for the cruises, and the Captains and the crews of the R/V New Horizon, R/V David Starr Jordan, and R/V Robert Gordon Sproul for their expert execution of the CalCOFI and red tide cruises.

References

Ahn, Y.-H., A. Bricaud, and A. Morel, Light backscattering efficiency and related properties of some phytoplankters, *Deep Sea Res., Part A, 39,* 1835-1855, 1992.

Aiken, J., G.F. Moore, C.C. Trees, S.B. Hooker, and D.K. Clark, SeaWiFS CZCS - type pigment algorithm, in SeaWiFS Technical Report Series, vol. 29, edited by S.B. Hooker and E.R. Firestone, NASA Tech. Memo. 104566, NASA, Greenbelt, Md., 1995.

Allen, W.E., "Red Water" in La Jolla Bay in 1946, *Trans. Am. Micros. Soc., 65,* 149-153, 1946.

Anderson, D.M., ECOHAB: The ecology and oceanography of harmful algal blooms: A national research agenda., 66 pp., Woods Hole Oceanogr. Inst., Woods Hole, Mass., 1995.

Austin, R.W., Inherent spectral radiance signatures of the ocean surface, in *Ocean Color Analysis*, edited by S.W. Duntley et al., *SIO ref. 74-10*, pp. 1-20, Univ. of Calif. San Diego, San Diego, Ca. 1974.

Balch, W.M., P.M. Holligan, S.G. Ackleson, and K.J. Voss, Biological and optical properties of mesoscale coccolithophore blooms in the Gulf of Maine, *Limnol. Oceanogr., 36,* 629-643, 1991.

Borstad, G.A., E.J. Carpenter, and J.F.R. Gower, Development of algorithms for remote sensing of *Trichodesmium* blooms., in *Marine Pelagic Cyanobacteria: Trichodesmium and other Diazotrophs*, edited by E.J. Carpenter, D.G. Capone and J.G. Rueter pp. 193-210, Kluwer Acad. Norwell, Mass., 1992.

Bricaud, A., M. Babin, A. Morel, and H. Claustre, Variability in the chlorophyll-specific absorption coefficients of natural phytoplankton: Analysis and parameterization, *J. Geophys. Res., 100,* 13,321-13,332, 1995.

Dunlap, W.C., B.E. Chalker, and J.K. Oliver, Bathymetric adaptations of reef-building corals at Davies Reef, Great Barrier Reef, Australia., III., UV-B absorbing compounds, *J. Exp. Mar. Biol. Ecol., 104,* 239-248, 1986.

Garver, S.A., D.A. Siegel, and B.G. Mitchell, Variability in near surface particulate absorption spectra: What can a satellite ocean color imager see? *Limnol. Oceanogr., 39,* 1349-1367, 1994.

Gordon, H.R., and K. Ding, Self-shading of in-water optical instruments, *Limnol. Oceanogr., 37,* 491-500, 1992.

Gordon, H.R., and A. Morel, *Remote Assessment of Ocean Color for Interpretation of Satellite Visible Imagery; A Review: Lecture Notes on Coastal and Estuarine Studies.*, 114 pp., Springer-Verlag, New York, 1983.

Gordon, H.R., O.B. Brown, R.H. Evans, J.W. Brown, R.C. Smith, K.S. Baker, D.K. Clark. A semianalytic radiance model of ocean color, *J. Geophys. Res., 93,* 10,909-10,924, 1988.

Holmes, R.W., P.M. Williams, and R.W. Eppley, red water in La Jolla Bay, 1964-1966, *Limnol. Oceanogr., 12,* 503-512, 1967.

Holm-Hansen, O., C.J. Lorenzen, R.W. Holmes, and J.D.H. Strickland, Fluorometric determination of chlorophyll, *J. Cons. Int. Explor. Mer., 30,* 3-15, 1965.

Kahru, M., U. Horstmann, and O. Rud, Satellite detection of increased cyanobacteria blooms in the Baltic Sea: Natural fluctuation or ecosystem change?, *Ambio, 23,* 469-472, 1994.

Kirk, J.T.O., Volume scattering function, average cosines, and the underwater light field, *Limnol. Oceanogr.*, 36, 455-467, 1991.

Mitchell, B.G., Algorithms for determining the absorption coefficient of aquatic particulates using the quantitative filter technique (QFT), in *Ocean Optics X,* edited by R. Spinrad, pp. 137-148, Int. Soc. Opt. Eng., Bellingham, Wash., 1990.

Mitchell, B.G., and M. Kahru, Algorithms for SeaWiFS standard products developed with the CalCOFI bio-optical data set, *Cal. Coop. Ocean. Fish. Invest. Rept.* in press, 1998.

Mitchell, B.G., and D.A. Kiefer, Chlorophyll *a* specific absorption and fluorescence excitation spectra for light-limited phytoplankton, *Deep Sea Res., Part A, 35,* 639-663, 1988.

Morel, A., and B. Gentili, Diffuse reflectance of oceanic waters: Its dependence on Sun angle as influenced by the molecular scattering contribution, *Appl. Opt., 30,* 4427-4438, 1991.

Morel, A., and B. Gentili, Diffuse reflectance of oceanic waters., III., Implications of bidirectionality for the remote-sensing problem, *Appl. Opt., 35,* 4850-4862, 1996.

Mueller, J.L., and R.W. Austin, Ocean optics protocols for SeaWiFS validation, Revision 1, in SeaWiFS Technical Report Series, vol. 25, NASA Tech. Memo. 104566, NASA, Greenbelt, Md., 1995.

Neale, P.J., A.T. Banaszak, and C. Jarriel, UV photoprotection by mycosporine-like amino acids is spectrally specific in *Gymnodinium sanguineum,* paper presented at 1997 Aquatic Science Meeting, Am. Soc. Limnol. and Oceanogr., Santa Fe, NM, 1997.

O'Reilly, J.E., S. Maritorena, B.G. Mitchell, D.A. Siegel, K.L. Carder, S.A. Garver, M. Kahru, and C.R. McClain, Ocean color chlorophyll algorithms for SeaWiFS, *J. Geophys. Res.*, in press, 1998.

Pegau, W.S., and J.R.V. Zaneveld, Temperature-dependent absorption of water in the red and near infrared portions of the spectrum, *Limnol. Oceanogr., 38,* 188-192, 1993

Siegel, D.A., and A.F. Michaels, Quantification of non-algal light attenuation in the Sargasso Sea: Implications for biogeochemistry and remote sensing, *Deep Sea Res., Part II, 43,* 321-345, 1996.

Siegel, D.A., M.C. O'Brien, J.C. Sorensen, D.A. Konnoff, and E. Fields, BBOP Data Processing and Sampling Procedures, Planning and Coordination Rept. #19, 77 pp., U.S. Joint Global Ocean Flux Study Planning and Coordination Office, Woods Hole Oceanographic Institution, Woods Hole, Mass., 1995.

Sosik, H.M., and B.G. Mitchell, Light absorption by phytoplankton, photosynthetic pigments, and detritus in the California Current System, *Deep Sea Res., Part A, 42,* 1717-1748, 1995.

Torrey, H.B., An Unusual occurrence of dinoflagellata on the California coast, *Am. Nat., 36,* 187-192, 1902.

Venrick, E.L., and T.L. Hayward, Determining chlorophyll on the 1984 CalCOFI surveys, *Rep. XXV, pp.* 74-79, Calif. Coop. Ocean. Fish. Invest., La Jolla, 1984.

Vernet, M., and K. Whitehead, Release of ultraviolet-absorbing compounds by the red-tide dinoflagellate *Gonyaulax polyedra, Mar. Biol., 127,* 35-44, 1996.

Vernet, M., E.A. Brody, O. Holm-Hansen, and B.G. Mitchell, The response of Antarctic phytoplankton to ultraviolet light: Absorption, photosynthesis, and taxonomic composition, *Antarct. Res. Ser., 62,* 143-158, 1994.

Zibordi, G., and G.M. Ferrari, Instrument self shading in underwater optical measurements: Experimental data, *Appl. Opt., 34,* 2750-2754, 1995.

M. Kahru and B.G. Mitchell, Scripps Institution of Oceanography, University of California San Diego, La Jolla, CA 92093-0218. (e-mail: mkahru@ucsd.edu; gmitchell@ucsd.edu)

(Received October 23, 1997; revised May 11, 1998; accepted June 5, 1998.)